AGU100 ADVANCING EARTH AND SPACE SCIENCE

Earth and Space Science

TECHNICAL REPORTS: METHODS
10.1029/2018EA000539

A Simple Method for Extracting Water Depth From Multispectral Satellite Imagery in Regions of Variable Bottom Type

Emily C. Geyman[1] **and Adam C. Maloof**[1]

[1]Department of Geosciences, Princeton University, Princeton, NJ, USA

Key Points:
- We use satellite imagery to estimate water depth on the Great Bahama Bank with 0.2-m accuracy
- Our algorithm is more robust to variable bottom types than the widely used linear and ratio methods
- Our physics-based method outperforms the support vector machines (SVM) algorithm in cases of limited calibration data coverage

Supporting Information:
- Supporting Information S1
- Data Set S1
- Data Set S2
- Data Set S3
- Data Set S4
- Data Set S5

Correspondence to:
E. C. Geyman,
egeyman@princeton.edu

Citation:
Geyman, E. C., & Maloof, A. C. (2019). A simple method for extracting water depth from multispectral satellite imagery in regions of variable bottom type. *Earth and Space Science*, *6*, 527–537. https://doi.org/10.1029/2018EA000539

Received 16 DEC 2018
Accepted 15 FEB 2019
Accepted article online 23 FEB 2019
Published online 30 MAR 2019

Abstract Satellite imagery offers an efficient and cost-effective means of estimating water depth in shallow environments. However, traditional empirical algorithms for calculating water depth often are unable to account for varying bottom reflectance, and therefore yield biased estimates for certain benthic environments. We present a simple method that is grounded in the physics of radiative transfer in seawater, but made more robust through the calibration of individual color-to-depth relationships for separate spectral classes. Our cluster-based regression (CBR) algorithm, applied to a portion of the Great Bahama Bank, drastically reduces the geographic structure in the residual and has a mean absolute error of 0.19 m with quantified uncertainties. Our CBR bathymetry is 3–5 times more accurate than existing models and outperforms machine learning protocols at extrapolating beyond the calibration data. Finally, we demonstrate how comparison of CBR with traditional models sensitive to bottom type reveals the characteristic length scales of biosedimentary facies belts.

1. Introduction

Obtaining an accurate bathymetry is an essential first step in any study of coastal processes such as estuarine circulation, sediment transport, delta morphology, and reef ecology. Historically, bathymetric data were acquired from depth soundings made by boats. However, boat-based measurements limited accurate estimates of seafloor topography to ship tracks and left shallow and remote waters unsampled. The advent of satellite radar altimetry measurements filled in our map of the global seafloor, but still left shallow regions poorly constrained (Calmant et al., 2002; Marks et al., 2010; Sandwell et al., 2006, 2014; Smith & Sandwell, 1997, 2004).

Airborne bathymetric LiDAR, which can achieve spatial resolutions of ≤1 m and vertical resolutions of ≤15 cm (Brock et al., 2004; Zawada & Brock, 2009), is emerging as the premier technology for creating high-resolution digital terrain models for coral reefs and other shallow-water environments (Brock et al., 2004; Costa et al., 2009; Pittman et al., 2013; Purkis & Kohler, 2008; Walker et al., 2008; Zawada & Brock, 2009). However, the cost of LiDAR is still prohibitive for large-scale surveys, although ICESat-2 might eventually make LiDAR bathymetry more accessible (Forfinski-Sarkozi & Parrish, 2016). Likewise, drones, coupled with structure-from-motion (SfM) and fluid lensing technology (Chirayath & Earle, 2016) enable bathymetric mapping at centimeter-scale resolution (Casella et al., 2017; Hamylton, 2017; Purkis, 2018). However, drone surveys are restricted to relatively small areas due to the battery limitations of quadcopters and fixed-wing unmanned aerial vehicles. Bathymetric estimates based on multispectral satellite imagery offer an essential complement to sonar-, gravity-, drone-, and LiDAR-derived estimates due to their low cost, relatively high spatial and temporal resolution, and wide coverage, including regions that are inaccessible to hydrographic vessels.

All algorithms for extracting water depth from satellite imagery are based on the simple physical principle that water attenuates light. Broadly, bathymetric algorithms can be grouped into two categories: empirical methods, which use direct observations of water depth in the study area to calibrate the reflectance-to-depth relationship, and physics-based inversion algorithms that use radiative transfer models to solve for water depth without in situ calibration data (Adler-Golden et al., 2005; Albert & Gege, 2006; Brando et al., 2009; Kerr & Purkis, 2018; Lee et al., 1998, 1999; Maritorena et al., 1994).

A major advantage of the physics-based methods—specifically, inversion algorithms based on spectral unmixing—is that they can derive water depth and seafloor reflectance simultaneously, making them robust to variations in bottom type (Bierwirth & Burne, 1993). However, physics-based inversion methods demand radiometric accuracy of the input satellite image—that is, they are highly sensitive to the atmospheric correction used to convert the total radiance received by the satellite to the transmitted radiance from the water column (Hedley et al., 2016; Vahtmae & Kutser, 2013). Atmospheric effects are significant; the transmitted radiance from the water column can represent as little as one quarter of the total radiance measured by the satellite sensor (Purkis, 2018). While correction schemes by Gordon (1997), Chavez (1988), and others effectively reduce atmospheric effects, the physics-based algorithms typically are unable to achieve depth estimates with root-mean-square errors less than ~1–2 m in shallow waters ≤20 m (Adler-Golden et al., 2005; Lyzenga et al., 2006).

Kerr and Purkis (2018) provide a bridge between the empirical and physics-based approaches, coupling forward modeling of the water column (Lee et al., 1999) with the ratio algorithm of Stumpf et al. (2003) that is widely applied in empirical studies. The model of Kerr and Purkis (2018) enables the estimation of water depths up to 15 m in tropical carbonate environments without the need for in situ water depth measurements as calibration data, an important result considering that the lack of ground truth data often is the primary obstacle for estimating bathymetry in shallow-water environments. An application of the Kerr and Purkis (2018) method to RapidEye imagery from Andros Island yields a root-mean-squared error of of 1.43 m in regions shallower than 15 m (Kerr & Purkis, 2018). However, our application of parsing the relationship between biosedimentary facies and water depth demands elevation precision on the order of tens of centimeters rather than meters (Maloof & Grotzinger, 2012). Moreover, our extensive set of ground truth data (Figure 1) affords a more precise model than the robust but relatively coarse model of Kerr and Purkis (2018).

Lyzenga, (1978, 1981) proposed a basic algorithm for calculating water depth from satellite imagery based on the Beer-Lambert Law of Absorption, which specifies a log-linear relationship between reflectance and water depth. Due to its efficacy and simplicity, the Lyzenga method has been adapted and widely applied to the bathymetric mapping of shallow marine environments (Bierwirth & Burne, 1993; Clark et al., 1987; Dierssen et al., 2003; Figueiredo et al., 2016; Hogrefe, Wright, & Hochberg, 2008; Hogrefe et al., 2008; Kanno et al., 2013; Liang et al., 2017; Lyons et al., 2011; Lyzenga, 1985; Lyzenga et al., 2006; Manessa et al., 2014; Misra et al., 2018; Mumby et al., 1998; O'Neill & Miller, 1989; Paredes & Spero, 1983; Philpot, 1989; Polcyn et al., 1970; Spitzer & Dirks, 1987).

A major drawback of the linear algorithm developed by Lyzenga, (1978, 1981) is that it assumes a uniform bottom albedo. As a result, depth estimates for particular benthic environments may be biased. One attempt at deriving a depth estimate that is independent of bottom type is to use the *ratio* of reflectance for two different spectral bands (Clark et al., 1987; Kerr & Purkis, 2018; Mumby et al., 1998; Paredes & Spero, 1983; Stumpf et al., 2003). Because the rate of light attenuation in water is wavelength dependent, the ratio of reflectance for two different wavelengths is a function of water depth and, in theory, less sensitive to bottom albedo. However, authors have had limited success applying the ratio algorithm to regions with highly variable bottom type (Doxani et al., 2012; Lyons et al., 2011), inspiring some to use more complex methods such as artificial neural networks and machine learning techniques (Ceyhun & Yalcin, 2010; Eugenio et al., 2015; Gholamalifard et al., 2013; Liu et al., 2015; Makboul et al., 2017; Sandidge & Holyer, 1998).

We show that while the linear and ratio algorithms are unable to fully accommodate variable bottom types, they are more likely to produce reasonable depth estimates for regions outside the domain of the calibration data, since the linear and ratio algorithms are still grounded by the physics of radiative transfer in seawater (Lyzenga, 1978; Spitzer & Dirks, 1987; Stumpf et al., 2003). Nonlinear machine learning approaches such as support vector machines (SVM) fit complex surfaces to the calibration data, which, when extrapolated to points outside the domain of the calibration data, may yield highly inaccurate estimates. We propose a simple method that (1) represents an intermediate between the linear/ratio algorithms and machine learning approaches and (2) can be tailored to match the goals of a mapping campaign—for example, to precisely describe the bathymetry in the region for which there are calibration data or to use a small number of ground-truthing points to predict water depth over a much larger region.

Our *cluster-based regression* (CBR) algorithm first segments the satellite image into zones of spectral homogeneity, and then calibrates the log-linear color-to-depth relationship separately for each class. The CBR

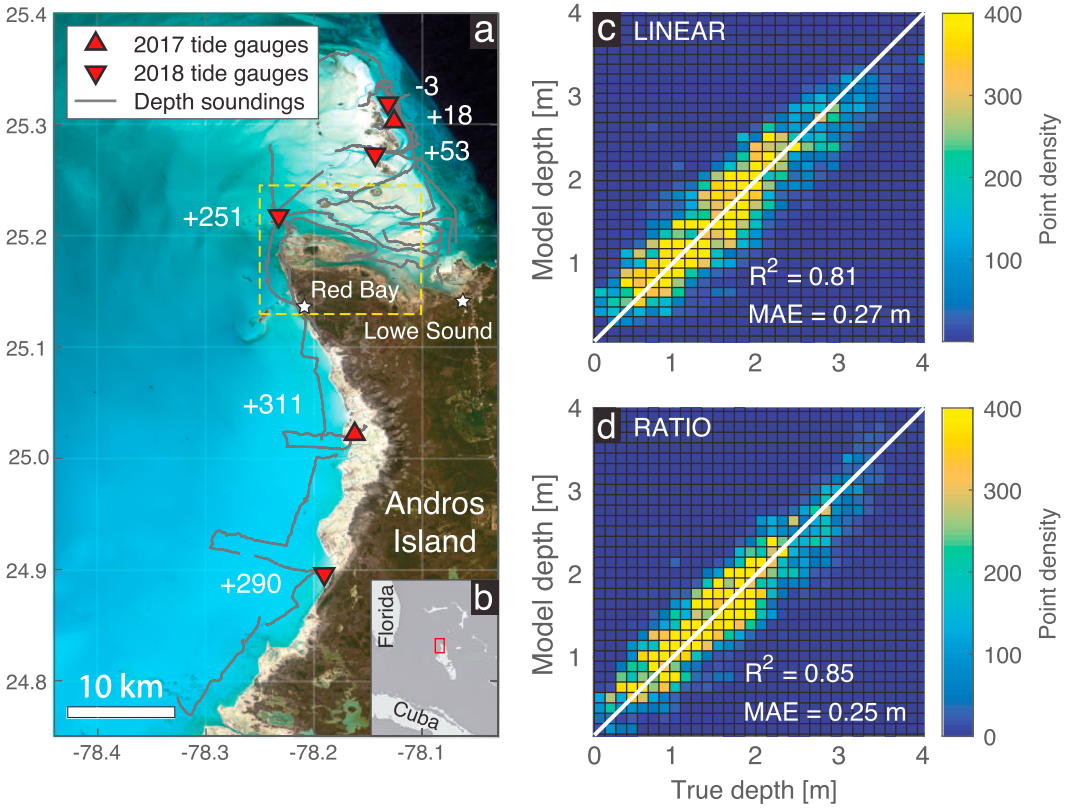

Figure 1. (a) RapidEye acquisition of the Great Bahama Bank in the region NW of Andros Island. The RapidEye image (16 March 2018) has a pixel resolution of 5.0 m and measures reflectance in five chromatic bands: blue, green, red, red edge, and NIR. Because only the blue, green, and red bands have good penetration in the water column, other satellites such as WorldView-2 and WorldView-3 that have more water-penetrating spectral bands could yield tighter color-to-depth relationships via equation (4). The gray lines depict the locations of 225,131 depth soundings from the acoustic surveys. The tidal lags (in minutes) of each tide gauge relative to the station at Fresh Creek, Andros Island are shown in white. The yellow outline denotes the region in Figure 4a. (b) The red box in the inset is the area of not only Figure 1a, but also Figures 2c, 2d, and 3. True depth versus model depth for simple extensions of the traditional (c) linear and (d) ratio algorithms. We use a multiple linear regression to combine the log-linear color-to-depth relationships from several spectral bands in the satellite image (equations (2) and (4)). The white line has slope 1 and represents perfect agreement between the true and model depths.

algorithm applies an extension of the Stumpf et al. (2003) ratio method that uses multiple band ratios (rather than just one) to leverage more information from the satellite image (Kerr & Purkis, 2018). The CBR model reduces bias and error, quantifies depth uncertainty, diminishes the geographic structure of the residual, and enables more accurate estimation of water depth over a wide variety of bottom types. We apply the CBR algorithm to the shallow waters on a portion of the Great Bahama Bank (Figure 1a), where the relationship between water depth and bottom type may be the key to understanding how to interpret sea level change from the rock record of carbonate stratigraphy (Dyer et al., 2018). Comparison of the residual from CBR and the standard linear model reveals the characteristic length scales of unique spectral lithotopes in this region of the Great Bahama Bank, and may be highlighting the impact of biosedimentary facies belts on bottom albedo.

2. Data and Methods

2.1. Field Surveys and Tidal Correction

We calibrate the relationship between water depth and color in a RapidEye satellite image (Figure 1a) using a total of 225,131 depth soundings acquired with a BioSonics MX Aquatic Habitat Echosounder (single frequency, 204.8 kHz). We deployed the echosounder during two 3-week field surveys in June 2017 and June 2018. Because the mean observed tidal range (~0.8 m) is large relative to the average depth in the acoustic survey (~1.6 m), we correct all depth measurements for their spatiotemporal position in the

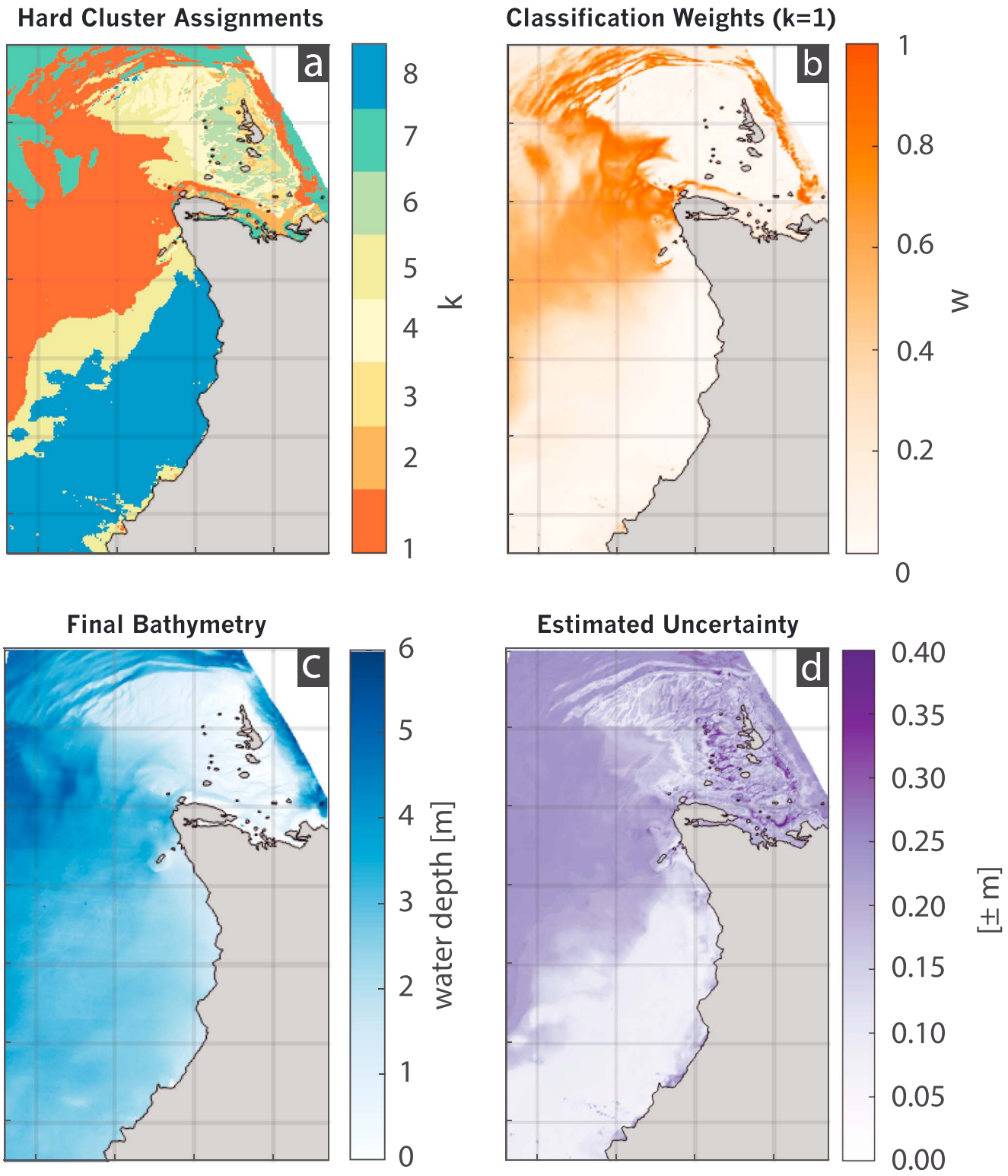

Figure 2. (a) Cluster assignments for a *k*-means classification of the RapidEye image (Figure 1) with $k = 8$. (b) Classification weights for cluster 1. (c) Final bathymetry, computed using the cluster-based regression algorithm. (d) Uncertainty associated with (c). Note that the uncertainty represents the *error bars* of the final bathymetry, not error (section 2.3). To obtain an additional estimate of uncertainty, we apply the cluster-based regression algorithm to seven different cloud-free RapidEye images (supporting information, Figure S3). The resulting depth estimates have standard deviations of ~0.25 m for the study area as a whole and ≤0.10 m in regions near calibration points (supporting information, Figure S4). The grid spacing is 0.1° of latitude/longitude (~11 km).

tidal cycle (Figure 1a). We zero-center the reflectance values for each spectral band before performing the color-to-depth regressions (e.g., Figures 1c and 1d), so linear atmospheric correction schemes such as dark object subtraction (Chavez, 1988, 1996) have no impact on our results.

2.2. Bathymetric Models

We apply four different algorithms for deriving water depth from color.

2.2.1. Linear Algorithm

The standard linear algorithm (Lyzenga, 1978) assumes a log-linear relationship between reflectance ($R(\lambda_i)$) and water depth (z):

$$z = b \log R(\lambda_i) + c \tag{1}$$

Often, the relationship between water depth and color is better constrained by using *several* bands (wavelengths) in multispectral satellite imagery (Lyons et al., 2011; Lyzenga, 1978; Stumpf et al., 2003). We combine the individual regressions for each wavelength (equation (1)) into a multiple linear regression:

$$z = \sum_{i=1}^{n} b_i \log R(\lambda_i) + c_i \tag{2}$$

where n is the number of spectral bands.

2.2.2. Ratio Algorithm

An important limitation of the linear algorithm (equation (2)) is that it does not account for changes in bottom type (e.g., a benthic environment covered in dark grass versus one covered in white sand—Figure 3). The ratio algorithm (equation (3)) is one attempt at deriving a depth estimate that is *independent* of bottom reflectance (Stumpf et al., 2003):

$$z = m \frac{\log R(\lambda_i)}{\log R(\lambda_j)} + c \tag{3}$$

where $R(\lambda_i)$ and $R(\lambda_j)$ are the reflectance in bands i and j, respectively. As with the linear algorithm, we can leverage information from all n spectral bands in the satellite image by extending equation (3) to a multiple linear regression:

$$z = \sum_{i=1}^{n} \sum_{j=1}^{n} m_{ij} \frac{\log R(\lambda_i)}{\log R(\lambda_j)} + c_{ij} \tag{4}$$

where $i \neq j$. In a five-band multispectral satellite image (Figure 1), there are 20 possible band ratios, some of which have stronger correlations with water depth than others. We perform a variance reduction analysis to determine that B3/B1 is the most effective band ratio, followed by B4/B1. Adding three more band ratios: B4/B3, B5/B2, and B5/B3 only slightly improves model performance. We should note that, because B5 (760–850 nm) does not penetrate the water column, the B5/B2 and B5/B3 ratios scale like 1/B2 and 1/B3. The specific selection of band ratios to use in equation (4) should be chosen on a site-specific basis. For example, in study areas with a deeper mean depth, bands 4 and 5 are unlikely to be useful as they are in the near infrared and cannot effectively penetrate the water column.

2.2.3. The CBR Method

The CBR method is equivalent to repeating the ratio algorithm (equation (4)) for different subsets of the image. Using a k-means unsupervised classification, we divide the RapidEye image into eight spectral classes (Figure 2a). Sensitivity analysis suggests that the final bathymetry is insensitive to the choice of k for $k =$ 4–12 (supporting information Figure S2), and Figure 5 depicts why we choose $k = 8$ for our data set. We use the depth soundings from within each spectral class to generate class-specific bathymetric models following equation (4). The final bathymetric estimate is a weighted mean of the eight bathymetric estimates, where the weights are the inverse spectral distances between a given pixel and each class centroid.

2.2.4. SVM Algorithm

We use a machine learning approach called support vector machines (SVM) as an alternative to the standard linear and ratio methods. Using the radial basis function kernel, we map the satellite color data to a high-dimensional feature space and then construct a regression hyperplane in this high-dimensional space. We implement SVM in MATLAB and perform Bayesian optimization with cross validation to solve for the three tunable parameters of the SVM regression: the box constraint, kernel scale, and epsilon.

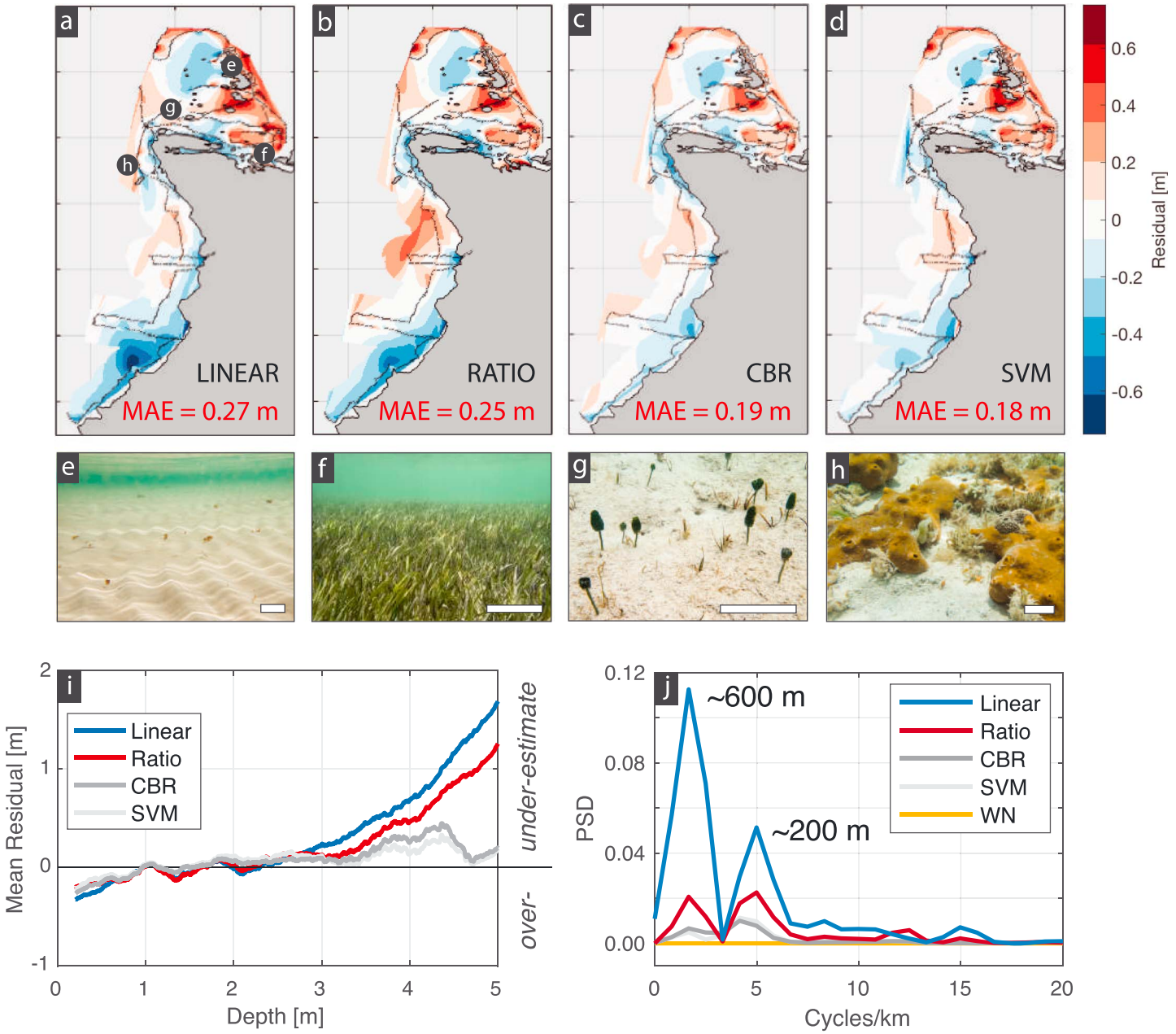

Figure 3. (a–d) Geographic patterns in the residual (true depth minus model depth) from depth estimates for the linear (a), ratio (b), CBR (c), and SVM (d) algorithms. Note that the CBR and SVM methods produce residuals with the least geographic structure. (e–h) The efficacy of the CBR and SVM methods is due to their robustness to different bottom types. Photos (e)–(h) illustrate a sampling of the diversity of bottom types observed around Andros Island. The white scale bars in each photo represent 5 cm. (i) Depth structure of the residual from the linear, ratio, CBR, and SVM algorithms. (j) Power spectral density of the variogram (variance as a function of lag distance) of the residuals in (a)–(d). The CBR and SVM residuals resemble white noise (WN), while the linear algorithm residuals have significant power around wavelengths of 600 and 200 m. CBR = cluster-based regression; SVM = support vector machines.

2.3. Quantifying Error in Bathymetric Models

To avoid overfitting, we partition the data set of 225,131 depth soundings (Figure 1a) into 60% used for model training, 20% for validation, and 20% for testing, a typical breakdown for machine learning studies (Kohavi, 1995; Parameswaran & Weinberger, 2010; Verrelst et al., 2012). Importantly, the segmentation of the original data set into training, validation, and testing sets enables us to evaluate bathymetric models on data that are not used for model calibration. To estimate uncertainty in the final bathymetry (Figure 2), we compute a weighted mean of the absolute errors of the $N = 20$ points in the testing set with the most similar spectral signatures to the pixel of interest. Sensitivity analysis reveals that the error estimate is insensitive

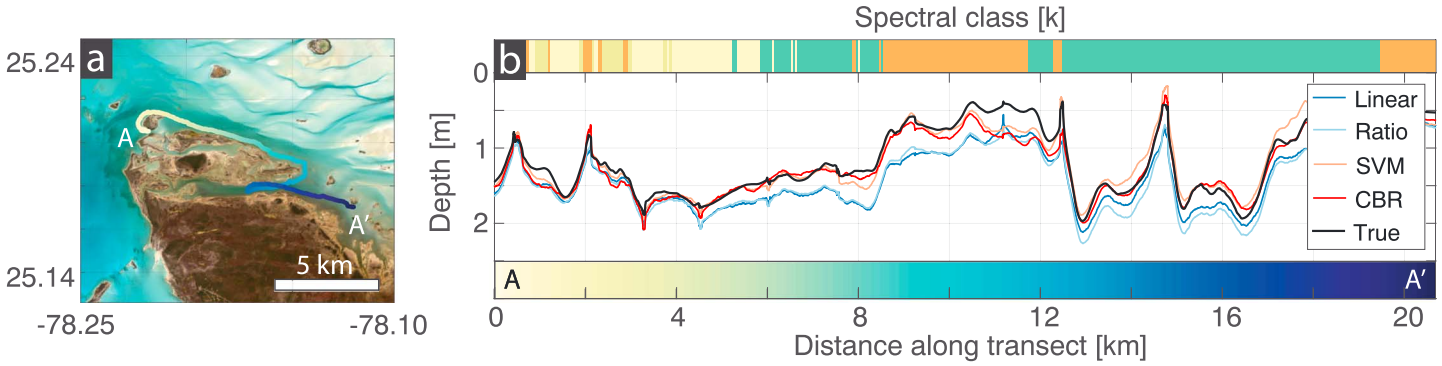

Figure 4. (a) An example 20-km transect of depth soundings around the NW corner of Andros Island (Figure 1). (b) Depth estimates along the transect generated by the linear, ratio, SVM, and CBR methods. The true (measured) depths are denoted in black. The spectral class assignments (k) along the transect follow the same color scheme as in Figure 2a. Notice that for class 4 (yellow), all four algorithms produce reasonable depth estimates. However, from 6–12 km along the transect, the linear and ratio algorithms significantly overestimate depth for classes 7 (green) and 2 (orange), which both correspond to relatively dark benthic environments (e.g., sea grass and dark sediment). Between 10 and 12 km, even the CBR and SVM methods overestimate depth, likely due to the unique presence of dark gray sediment in that region (as opposed to the white sediment elsewhere—Figures 3e–3h), which is not spatially extensive enough to constitute its own *k*-means spectral class. CBR = cluster-based regression; SVM = support vector machines.

to the choice of N. Additionally, as a test of model sensitivity, we apply the CBR algorithm to seven different cloud-free RapidEye scenes and study the variability of the resulting bathymetric estimates (supporting information, Figure S4).

3. Results

The linear and ratio algorithms produce reliable depth estimates with mean absolute errors (MAEs) of 0.27 and 0.25 m, respectively (Figures 1c and 1d). However, both algorithms significantly underestimate depth in waters deeper than about 3 m (Figure 3i). Residuals of the linear and ratio depth estimates also show significant geographic structure (Figures 3a and 3b), suggesting that the two algorithms are not robust to varying bottom reflectance from the diversity of benthic habitats observed on the Great Bahama Bank (Figures 3e–3h). The CBR and SVM algorithms not only have smaller MAEs (0.19 and 0.18 m, respectively) but also produce residuals with less geographic and depth structure (Figure 3).

4. Discussion

4.1. Dependence of Depth Estimate on Bottom Type

The significant geographic structure of the linear and ratio method residuals (Figures 3a and 3b) suggests that those methods are not robust to variable bottom type. Do the CBR and SVM approaches produce accurate depth estimates even when the spectral properties of the seafloor change? In the example acous-

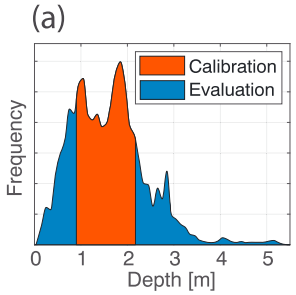

(b)

Algorithm	1 Random	2 Geography	3 Depth	4 Color
Linear	0.27	0.36	0.59	0.43
Ratio	0.25	0.30	0.57	0.37
CBR ($k = 3$)	0.22	0.29	0.57	0.34
CBR ($k = 4$)	0.21	0.28	0.52	0.45
CBR ($k = 8$)	0.19	0.24	0.52	0.58
SVM	0.18	0.29	0.95	0.59

Figure 5. Mean absolute errors, reported in meters, for the linear, ratio, CBR, and SVM algorithms in four different experiments. In all cases, the bathymetric models are trained on 60% of the data set and evaluated on the remaining 40%. In (b1), the data set is partitioned randomly into the calibration and evaluation sets. In (b2), the data are calibrated using the middle 60% of all measured water depths and evaluated on the shallowest and deepest parts of the data set, as depicted in (a). In (b3) and (b4), the data are trained on the middle 60% of the data set, defined in terms of distance to the spectral and geographic centroids, respectively. The CBR method performs like the ratio method for small k and SVM for large k. We use $k = 8$ classes in the final bathymetric model (Figure 2a).

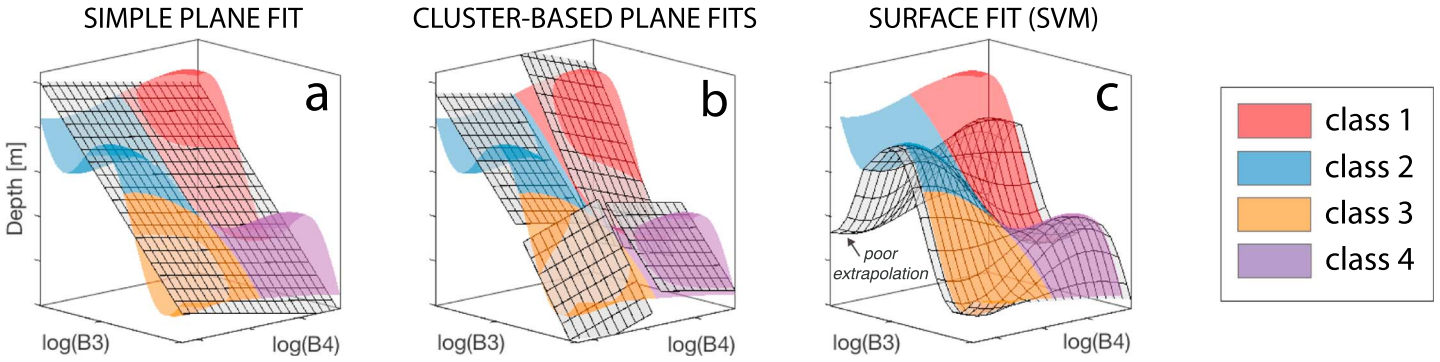

Figure 6. A cartoon comparing the linear and ratio algorithms (a) to CBR (b) and SVM (c). The colored surface represents the complex mapping between image color and water depth. The black and white gridded surface represents the model fit. Although the RapidEye image (Figure 1) has 5 spectral bands, for simplicity we depict just the two bands with the strongest color-to-depth correlations (bands 3 and 4).

tic survey transect in Figure 4, the CBR and SVM algorithms consistently match the measured depth, while the linear and ratio algorithms overestimate depth when the spectral class (Figure 2a) switches from predominantly class 4 to classes 2 and 7.

4.2. Extrapolating Beyond the Domain of the Calibration Data Set

Due to the high cost of acoustic field surveys and the inaccessibility of very shallow waters, it is common for calibration data to incompletely cover the region of interest. An ideal bathymetric model is one that not only matches the calibration data precisely but also provides robust estimates for areas one cannot visit. As a test of model performance, we conduct an experiment in which we train each bathymetric model on the central 60% of the data set defined in terms of geography, water depth or color and then evaluate the trained model on the remaining 40% of the data set (Figure 5).

SVM has the worst extrapolation error for color and water depth (Figure 5). Meanwhile, linear and ratio models perform the best when extrapolating to pixels with colors outside the domain of the calibration data set (Figure 5).

4.3. Cluster-Based Method as an Intermediate Between the Linear/Ratio Algorithms and SVM

Figure 6 conceptualizes the relationship between the linear/ratio, CBR, and SVM algorithms. In the idealized case of a uniform seafloor, water depth should be a linear function of $\log(R(\lambda_i))$ (Lyzenga, 1978). In other words, in three dimensions, there should be a plane mapping $\log(R(\lambda_i))$ for two bands in a satellite image to water depth. In reality, variable bottom reflectance due to different benthic habitats (Figure 3) influence the color-to-depth relationship, leading to a complex surface like the one depicted in Figure 6. The simple linear algorithm seeks to fit the surface with a single plane. Meanwhile, the CBR method partitions the surface into different zones based on spectral class and then fits each zone with a separate plane. Finally, SVM attempts to fit the entire surface (Figure 6).

A danger of SVM compared to the linear, ratio, and CBR algorithms that are rooted in the physical principle of the log-linear relationship between reflectance and water depth is that the SVM performs poorly when forced to extrapolate beyond the range of the calibration data set (Figures 5 and 6). The CBR approach represents a compromise between the two end-members of fitting the complex surface in Figure 6 with a single hyperplane or using SVM to fit the whole surface. As we increase the number of spectral classes (k) in the CBR method, we move between the two end-member scenarios—using a single spectral class is equivalent to the standard ratio method and using many spectral classes begins to approximate SVM (Figure 5).

4.4. Geographic Correlation Structure of the Residual and Length Scales of Bottom-Type Variability

The most important feature of CBR and SVM is their reduction in the geographic correlation structure of the residual (Figure 3). The Fourier transform of the semivariance (Figure 3j) shows that, while even our best models cannot completely remove the effects of bottom type, CBR and SVM produce residuals that resemble white noise more than the traditional algorithms. In contrast, the linear method, which is most sensitive to bottom-type variability, yields residuals with power at wavelengths of 200 and 600 m, suggesting that those

are the dominant length scales of biosedimentary facies belts that control bottom albedo in this region of the Great Bahama Bank.

4.5. Water Depth and Sedimentary Facies

Our CBR method produces depth estimates with a mean absolute error of 0.19 m (17% error) and an R^2 value of 0.90. In contrast, the best existing bathymetric map of the Great Bahama Bank (Harris et al., 2015), which is based on an interpolation of published depth soundings—as few as 11 of which are in the region in Figure 1—yields a mean absolute error of 0.59–0.69 m (53–62%) and an R^2 value of just 0.33 for the area of interest (Figure 1).

By quantifying the relationship between water depth and bottom type (*biosedimentary facies*) in modern shallow-water carbonate environments like the Bahamas, we can improve our interpretations of ancient sea level from carbonate stratigraphy (Dyer et al., 2018). However, the link between water depth and facies is subtle and noisy (Harris et al., 2014, 2015; Purkis et al., 2012, 2014). As an extreme example, Maloof and Grotzinger (2012) showed that the entire elevation range of intertidal facies on the west side of Andros Island is only about 0.6 m. Our high-resolution bathymetry with quantified uncertainty (Figures 2c and 2d), which is available for download in the supporting information, enables the investigation of facies-depth relationships at vertical scales as small as 0.2 m.

5. Conclusions

We use RapidEye satellite imagery and four algorithms to estimate water depth on a portion of the Great Bahama Bank. We show that the linear and ratio algorithms are unable to accommodate the nonlinearities in the empirical color-to-depth relationships caused by variable bottom type, but provide robust estimates for waters shallower or deeper than those sampled in the calibration data set, since the log-linear relationship between color and depth is based on physics. In contrast, the nonlinear SVM algorithm may yield tighter fits of the calibration data, but is unlikely to produce satisfactory results if the calibration data set is not representative of the entire image. We offer the CBR method as a simple, flexible, and effective compromise between the linear/ratio and SVM algorithms.

Acknowledgments

Thank you to Jeff Birch at Small Hope Bay Lodge for making work possible on Andros Island. Also, thank you to Alex Cartwright, Rudolph "Timer" Coakley, Niki Hinsey, Anastasia Mackey, Alvin Marshall, Sonny "Abba" Martin, Bhruna Neymor, Garnet Thompson, Linda Whyms, and local customs and immigration. Chris Allen at Air Flight Charters and Dawn Reading at Princeton provided logistical support. Thank you to Liam O'Connor and Tano Humes for assistance in the field. Planet provided the RapidEye satellite imagery through the Planet Research Ambassadors Program (Planet Team, 2017). Thank you especially to Joe Mascaro at Planet. Frederik Simons offered helpful suggestions about how to probe the spatial correlation structure of the residual. Comments from S. J. Purkis significantly improved the manuscript. This material is based upon work supported by the Princeton Environmental Institute at Princeton University through the Smith-Newton Scholars Program. This work also was supported by the GSA Northeastern Section Stephen G. Pollock Undergraduate Student Research Grant, the Evolving Earth Foundation, the High Meadows Foundation, and the Sigma Xi Research Society. Georeferenced tiff images of the final bathymetry and uncertainty maps (Figures 2c and 2d), the median and standard deviation of the bathymetric maps obtained from seven different RapidEye acquisitions (supporting information, Figure S4), and a table containing the GPS coordinates and tide-corrected depths from the acoustic survey (Figure 1), are available in the supporting information.

References

Adler-Golden, S. M., Acharya, P. K., Berk, A., Matthew, M. W., & Gorodetzky, D. (2005). Remote bathymetry of the littoral zone from AVIRIS, LASH, and QuickBird imagery. *IEEE Transactions on Geoscience and Remote Sensing*, *43*(2), 337–347.

Albert, A., & Gege, P. (2006). Inversion of irradiance and remote sensing reflectance in shallow water between 400 and 800 nm for calculations of water and bottom properties. *Applied Optics*, *45*(10), 2331–2343.

Bierwirth, P., & Burne, R. V. (1993). Shallow sea-floor reflectance and water depth derived by unmixing multispectral imagery. *Photogrammetric Engineering & Remote Sensing*, *59*(3), 331–338.

Brando, V. E., Anstee, J. M., Wettle, M., Dekker, A. G., Phinn, S. R., & Roelfsema, C. (2009). A physics based retrieval and quality assessment of bathymetry from suboptimal hyperspectral data. *Remote Sensing of Environment*, *113*(4), 755–770.

Brock, J. C., Wright, C. W., Clayton, T. D., & Nayegandhi, A. (2004). Lidar optical rugosity of coral reefs in Biscayne National Park, Florida. *Coral Reefs*, *23*(1), 48–59.

Calmant, S., Berge-Nguyen, M., & Cazenave, A. (2002). Global seafloor topography from a least-squares inversion of altimetry-based high-resolution mean sea surface and shipboard soundings. *Geophysical Journal International*, *151*(3), 795–808.

Casella, E., Collin, A., Harris, D., Ferse, S., Bejarano, S., Parravicini, V, et al. (2017). Mapping coral reefs using consumer-grade drones and structure from motion photogrammetry techniques. *Coral Reefs*, *36*(1), 269–275.

Ceyhun, O., & Yalcin, A. (2010). Remote sensing of water depths in shallow waters via artificial neural networks. *Estuarine, Coastal and Shelf Science*, *89*(1), 89–96.

Chavez, P. S. (1988). An improved dark-object subtraction technique for atmospheric scattering correction of multispectral data. *Remote Sensing of Environment*, *24*(3), 459–479.

Chavez, P. S. (1996). Image-based atmospheric corrections—Revisited and improved. *Photogrammetric Engineering & Remote Sensing*, *62*(9), 1025–1036.

Chirayath, V., & Earle, S. A. (2016). Drones that see through waves—Preliminary results from airborne fluid lensing for centimetre-scale aquatic conservation. *Aquatic Conservation: Marine and Freshwater Ecosystems*, *26*(S2), 237–250.

Clark, R. K., Fay, T. H., & Walker, C. L. (1987). Bathymetry calculations with Landsat 4 TM imagery under a generalized ratio assumption. *Applied Optics*, *26*(19), 331–338.

Costa, B. M., Battista, T. A., & Pittman, S. J. (2009). Comparative evaluation of airborne LiDAR and ship-based multibeam SoNAR bathymetry and intensity for mapping coral reef ecosystems. *Remote Sensing of Environment*, *113*(5), 1082–1100.

Dierssen, H. M., Zimmerman, R. C., Leathers, R. A., Downes, T. Valerie, & Davis, C. O. (2003). Ocean color remote sensing of seagrass and bathymetry in the Bahamas Banks by high-resolution airborne imagery. *Limnology and Oceanography*, *48*, 444–455.

Doxani, G., Papadopoulou, M., Lafazani, P., Pikridas, C., & Tsakiri-Strati, M. (2012). Shallow-water bathymetry over variable bottom types using multispectral Worldview-2 image. *International Archives of the Photogrammetry, Remote Sensing and Spatial Information Sciences*, *XXXIX-B8*, 159–164.

Dyer, B., Maloof, A. C., Purkis, S. J., & Harris, P. M. (2018). Quantifying the relationship between water depth and carbonate facies. *Sedimentary Geology*, *373*, 1–10.
Eugenio, F., Marcello, J., & Martin, J. (2015). High-resolution maps of bathymetry and benthic habitats in shallow-water environments using multispectral remote sensing imagery. *IEEE Transactions on Geoscience and Remote Sensing*, *53*(7), 3539–3549.
Figueiredo, I. N., Pinto, L., & Goncalves, G. (2016). A modified Lyzenga's model for multispectral bathymetry using Tikhonov regularization. *IEEE Geoscience and Remote Sensing Letters*, *13*(1), 53–57.
Forfinski-Sarkozi, N. A., & Parrish, C. E. (2016). Analysis of MABEL bathymetry in Keweenaw Bay and implications for ICESat-2 ATLAS. *Remote Sensing*, *8*(9), 772.
Gholamalifard, M., Kutser, T., Esmaili-Sari, A., Abkar, A. A., & Naimi, B. (2013). Remotely sensed empirical modeling of bathymetry in the Southeastern Caspian Sea. *Remote Sensing*, *5*(6), 2746–2762.
Gordon, H. R. (1997). Atmospheric correction of ocean color imagery in the Earth observing system era. *Journal of Geophysical Research*, *102*, 17,081–17,106.
Hamylton, S. M. (2017). Mapping coral reef environments: A review of historical methods, recent advances and future opportunities. *Progress in Physical Geography: Earth and Environment*, *41*(6), 803–833.
Harris, P. M., Purkis, S. J., & Ellis, J. (2014). *Evaluating water-depth variation and mapping depositional facies on the Great Bahama Bank*. Tulsa, Okla: SEPM Society for Sedimentary Geology.
Harris, P. M., Purkis, S. J., Ellis, J., Swart, P. K., & Reijmer, J. (2015). Mapping bathymetry and depositional facies on the Great Bahama Bank. *Sedimentology*, *62*(2), 566–589.
Hedley, J. D., Roelfsema, C. M., Chollett, I., Harborne, A. R., Heron, S. F., Weeks, S., et al. (2016). Remote sensing of coral reefs for monitoring and management: A review. *Remote Sensing*, *8*(2), 118.
Hogrefe, K. R., Wright, D. J., & Hochberg, E. J. (2008). Derivation and integration of shallow-water bathymetry: Implications for coastal terrain modeling and subsequent analyses. *Marine Geodesy*, *31*(4), 299–317.
Kanno, A., Tanaka, Y., Kurosawa, A., & Sekine, M. (2013). Generalized Lyzenga's predictor of shallow water depth for multispectral satellite imagery. *Marine Geodesy*, *36*(4), 365–376.
Kerr, J. M., & Purkis, S. (2018). An algorithm for optically-deriving water depth from multispectral imagery in coral reef landscapes in the absence of ground-truth data. *Remote Sensing of Environment*, *210*, 307–324.
Kohavi, R. (1995). A study of cross-validation and bootstrap for accuracy estimation and model selection. In *International Joint Conference on Artificial Intelligence (IJCAI)*, *14*, Montreal, Canada, pp. 1137–1145.
Lee, Z., Carder, K. L., Mobley, C. D., Steward, R. G., & Patch, J. S. (1998). Hyperspectral remote sensing for shallow waters. I. A semianalytical model. *Applied Optics*, *37*(27), 6329–6338.
Lee, Z., Carder, K. L., Mobley, C. D., Steward, R. G., & Patch, J. S. (1999). Hyperspectral remote sensing for shallow waters: 2. Deriving bottom depths and water properties by optimization. *Applied Optics*, *38*(18), 3831–3843.
Liang, J., Zhang, J., Ma, Y., & Zhang, C.-Y. (2017). Derivation of bathymetry from high-resolution optical satellite imagery and USV sounding data. *Marine Geodesy*, *40*(6), 466–479.
Liu, S., Gao, Y., Zheng, W., & Li, X. (2015). Performance of two neural network models in bathymetry. *Remote Sensing Letters*, *6*(4), 321–330.
Lyons, M., Phinn, S., & Roelfsema, C. (2011). Integrating Quickbird multi-spectral satellite and field data: Mapping bathymetry, seagrass cover, seagrass species and change in Moreton Bay, Australia in 2004 and 2007. *Remote Sensing*, *3*(1), 42–64.
Lyzenga, D. R. (1978). Passive remote sensing techniques for mapping water depth and bottom features. *Applied Optics*, *17*(3), 379–383.
Lyzenga, D. R. (1981). Remote sensing of bottom reflectance and water attenuation parameters in shallow water using aircraft and Landsat data. *International Journal of Remote Sensing*, *2*(1), 71–82.
Lyzenga, D. R. (1985). Shallow-water bathymetry using combined lidar and passive multispectral scanner data. *International Journal of Remote Sensing*, *6*(1), 115–125.
Lyzenga, D. R., Malinas, N. P., & Tanis, F. J. (2006). Multispectral bathymetry using a simple physically based algorithm. *IEEE Transactions on Geoscience and Remote Sensing*, *44*(8), 2251–2259.
Makboul, O., Negm, A., Mesbah, S., & Mohasseb, M. (2017). Performance assessment of ANN in estimating remotely sensed extracted bathymetry. Case study: Eastern Harbor of Alexandria. *Procedia Engineering*, *181*, 912–919. 10th International Conference Interdisciplinarity in Engineering, INTER-ENG 2016, 6-7 October 2016, Tirgu Mures, Romania.
Maloof, A. C., & Grotzinger, J. P. (2012). The Holocene shallowing-upward parasequence of north-west Andros Island, Bahamas. *Sedimentology*, *59*, 1375–1407.
Manessa, M. D. M., Kanno, A., Sekine, M., Ampou, E. E., Widagti, N., & As-syakur, A. R. (2014). Shallow-water benthic identification using multispectral satellite imagery: Investigation on the effects of improving noise correction method and spectral cover. *Remote Sensing*, *6*(5), 4454–4472.
Maritorena, S., Morel, A., & Gentili, B. (1994). Diffuse reflectance of oceanic shallow waters: Influence of water depth and bottom albedo. *Limnology and Oceanography*, *39*(7), 1689–1703.
Marks, K. M., Smith, W. H. F., & Sandwell, D. T. (2010). Evolution of errors in the altimetric bathymetry model used by Google Earth and GEBCO. *Marine Geophysical Researches*, *31*(3), 223–238.
Misra, A., Vojinovic, Z., Ramakrishnan, B., Luijendijk, A., & Ranasinghe, R. (2018). Shallow water bathymetry mapping using support vector machine (SVM) technique and multispectral imagery. *International Journal of Remote Sensing*, *39*(13), 4431–4450.
Mumby, P. J., Clark, C. D., Green, E. P., & Edwards, A. J. (1998). Benefits of water column correction and contextual editing for mapping coral reefs. *International Journal of Remote Sensing*, *19*(1), 203–210.
O'Neill, N. T., & Miller, J. R. (1989). On calibration of passive optical bathymetry through depth soundings analysis and treatment of errors resulting from the spatial variation of environmental parameters. *International Journal of Remote Sensing*, *10*(9), 1481–1501.
Parameswaran, S., & Weinberger, K. Q. (2010). Large margin multi-task metric learning. In J. D. Lafferty, C. K. I. Williams, J. Shawe-Taylor, R. S. Zemel, & A. Culotta (Eds.), *Advances in neural information processing systems* (pp. 1867–1875). Vancouver, British Columbia, Canada: Curran Associates, Inc.
Paredes, J. M., & Spero, R. E. (1983). Water depth mapping from passive remote sensing data under a generalized ratio assumption. *Applied Optics*, *22*(8), 1134–1135.
Philpot, W. D. (1989). Bathymetric mapping with passive multispectral imagery. *Applied Optics*, *28*(8), 1569–1578.
Pittman, S. J., Costa, B., & Wedding, L. M. (2013). Lidar applications. In J. A. Goodman, S. J. Purkis, & S. R. Phinn (Eds.), *Coral reef remote sensing: A guide for mapping, monitoring and management* (pp. 145–174). Dordrecht: Springer Netherlands.
Planet Team (2017). Planet application program interface. In *Space for Life on Earth*. San Francisco, CA. Retrieved from https://api.planet.com
Polcyn, F. C., Brown, W. L., & Sattinger, I. J. (1970). The measurement of water depth by remote-sensing techniques (*8973-26-F*). Ann

Arbor, MI: Willow Run Laboratories, University of Michigan.
Purkis, S. J. (2018). Remote sensing tropical coral reefs: The view from above. *Annual Review of Marine Science*, *10*(1), 149–168.
Purkis, S. J., Harris, P. M., & Ellis, J. (2012). Patterns of sedimentation in the contemporary Red Sea as an analog for ancient carbonates in rift settings. *Journal of Sedimentary Research*, *82*, 859–870.
Purkis, S. J., & Kohler, K. E. (2008). The role of topography in promoting fractal patchiness in a carbonate shelf landscape. *Coral Reefs*, *27*(4), 977–989.
Purkis, S. J., Rowlands, G. P., & Kerr, J. M. (2014). Unravelling the influence of water depth and wave energy on the facies diversity of shelf carbonates. *Sedimentology*, *62*, 1–25.
Sandidge, J. C., & Holyer, R. J. (1998). Coastal bathymetry from hyperspectral observations of water radiance. *Remote Sensing of Environment*, *65*(3), 341–352.
Sandwell, D. T., Müller, R. D., Smith, W. H. F., Garcia, E., & Francis, R. (2014). New global marine gravity model from CryoSat-2 and Jason-1 reveals buried tectonic structure. *Science*, *346*(6205), 65–67.
Sandwell, D. T., Smith, W. H. F., Gille, S., Kappel, E., Jayne, S., Soofi, K., et al. (2006). Bathymetry from space: Rationale and requirements for a new, high-resolution altimetric mission. *Comptes Rendus Geoscience*, *338*(14), 1049–1062.
Smith, W. H. F., & Sandwell, D. T. (1997). Global sea floor topography from satellite altimetry and ship depth soundings. *Science*, *277*(5334), 1956–1962.
Smith, W. H. F., & Sandwell, D. T. (2004). Conventional bathymetry, bathymetry from space, and geodeticaltimetry. *Oceanography*, *17*, 8–23.
Spitzer, D., & Dirks, R. W. J. (1987). Bottom influence on the reflectance of the sea. *International Journal of Remote Sensing*, *8*(3), 279–308.
Stumpf, R. P., Holderied, K., & Sinclair, M. (2003). Determination of water depth with high-resolution satellite imagery over variable bottom types. *Limnology and Oceanography*, *48*(1), 547–556.
Vahtmae, E., & Kutser, T. (2013). Classifying the Baltic Sea shallow water habitats using image-based and spectral library methods. *Remote Sensing*, *5*(5), 2451–2474.
Verrelst, J., Muñoz, J., Alonso, L., Delegido, J., Rivera, J. P., Camps-Valls, G., & Moreno, J. (2012). Machine learning regression algorithms for biophysical parameter retrieval: Opportunities for Sentinel-2 and -3. *Remote Sensing of Environment*, *118*, 127–139.
Walker, B. K., Riegl, B., & Dodge, R. E. (2008). Mapping coral reef habitats in southeast Florida using a combined technique approach. *Journal of Coastal Research*, *24*, 1138–1150.
Zawada, D. G., & Brock, J. C. (2009). A multiscale analysis of coral reef topographic complexity using lidar-derived bathymetry. *Journal of Coastal Research*, *SI*, 6–15.